U.P.B. Sci. Bull., Series C, Vol. 88, Iss. 2, 2026 ISSN 2286 – 3540

COMPREHENSIVE POWER GENERATION SYSTEM BASED ON OPTIMIZED ANN FOR FULL SPECTRUM FREQUENCY DIVISION UTILIZATION OF SOLAR ENERGY

Xinyu KONG[1], Yongtong LI[2,*]

This article designs a new comprehensive power generation system for full spectrum cascade utilization, integrating frequency division and concentrated photovoltaic photothermal technology to construct a photovoltaic photothermal driven organic Rankine cycle power supply system, realizing power generation and hydrogen production through electrolysis of water. The potential for efficiency improvement is verified through theoretical modeling and thermodynamic analysis. Optimize artificial neural networks to solve the traditional gradient vanishing problem for photovoltaic module fault detection; By using MATLAB modeling to collect fault data and comparing it with KNN and LSTM, the diagnostic accuracy is higher, providing innovative ideas for system operation and photovoltaic intelligent operation and maintenance.

Keywords: Efficient use of solar energy; Frequency division technology; Concentrating photovoltaic photothermal; Optimized artificial neural network

1. Introduction

With the rapid development of the world economy, problems such as energy shortage and climate change have become prominent. The development and utilization of renewable energy have become the focus of global attention [1]. The latest report of the International Energy Agency (IEA) "global energy assessment 2025" shows that the new installed capacity of renewable energy climbed to about 700 GW in 2024, breaking the record for the 22nd consecutive year [2]. Renewable energy includes solar energy, wind energy, geothermal energy and Hydropower [3]. Among them, solar energy technology has attracted much attention due to its huge energy production potential.

In order to improve the photoelectric efficiency of photovoltaic cells, scholars designed a comprehensive utilization system of photovoltaic and thermal (PV/T). The system includes PV module and ST module. The photovoltaic cell converts the absorbed local solar radiation into electrical energy and completes the electrical energy output; The circulating working medium in the collector uses the flow to absorb the waste heat at the bottom of the battery and recover heat while

---

[1] Ms., College of Petrochemical Engineering, Lanzhou University of Technology, Lanzhou, Gansu 730050, China, e-mail: kxy202507@163.com

[2]* PhD, Associate Prof., College of Petrochemical Engineering, Lanzhou University of Technology, Lanzhou, Gansu 730050, China, Corresponding author, e-mail: Ly886604@126.com

cooling the battery [4]. Since the PV/T system was proposed by Professor wolf [5], many scholars have begun to carry out a lot of research on its material update, structural innovation, and excellent experimental work. Wangxiuyan[6] established the heat transfer mathematical model of the trough solar concentrator with high heat flux absorbed by one side, and found that the higher the solar radiation intensity, the higher the efficiency of the collector. Li et al. [7] proposed to laminate the photovoltaic cell to the back of the glass cover to improve the weakening of the electrical performance of the cell due to high temperature. Chae et al. [8] built a predictive numerical model to analyze the economic feasibility, energy performance and environmental impact of PV/T-ASHP system.Xiang Yuyue et al. [9] built a dual source heat pump hot water system based on PV/T, and selected four typical days in the year to test the reliability of the system, heat pump operation performance and PV/T operation characteristics.

This article adopts solar energy frequency division technology, which can reduce the heating of photovoltaic panels and concentrate the thermal energy after frequency division. Combined with a small working fluid flow rate, it can increase the inlet temperature of the expander, effectively improving the efficiency of solar energy utilization and power generation system. At the same time, research is being conducted on the synergistic utilization of photovoltaic and ORC to achieve solar power generation and drive hydrogen production in electrolytic cells through the use of photovoltaic and photothermal effects. In addition, an improved artificial neural network (ANN) detection method is proposed for photovoltaic module fault detection to solve the problem of gradient vanishing in existing ANN; Using MATLAB to establish a photovoltaic array simulation model and obtain simulation data, comparative analysis shows that this method has more advantages in diagnostic performance compared to the two machine learning methods in the literature.

2. System Design

The schematic diagram of integrated power supply system for full spectrum frequency division utilization of solar energy is shown in Fig 1, and the energy flow chart is shown in Fig 2, which mainly includes solar frequency division utilization/concentrating photovoltaic module, ORC system, PEM electrolyzer hydrogen production module.

1) Solar energy frequency division utilization/concentrating photovoltaic module: the module is composed of a reflective condenser, a frequency divider, a concentrating photovoltaic module, a photovoltaic cooling backplane, and a condenser and a photothermal collector. The core of the CPV module is a CPV panel, and a frequency divider is precisely arranged in front of the PV panel to

screen the light of a specific wavelength; A cooling plate is installed on the back of the photovoltaic panel to ensure that the battery works at a suitable temperature; The heat absorber surrounding the photovoltaic panel can effectively collect the light energy that cannot be projected onto the photovoltaic panel.

When the system is running, the sunlight is highly focused through the reflecting condenser to enhance the light energy density. Then, under the action of the frequency divider, the light within its allowable transmission wavelength is projected onto the surface of the photovoltaic panel to complete the photoelectric conversion; At the same time, the light of the remaining bands is reflected by the frequency divider, converged again through the condenser, and finally reaches the photothermal collector, which is converted into heat energy for utilization.

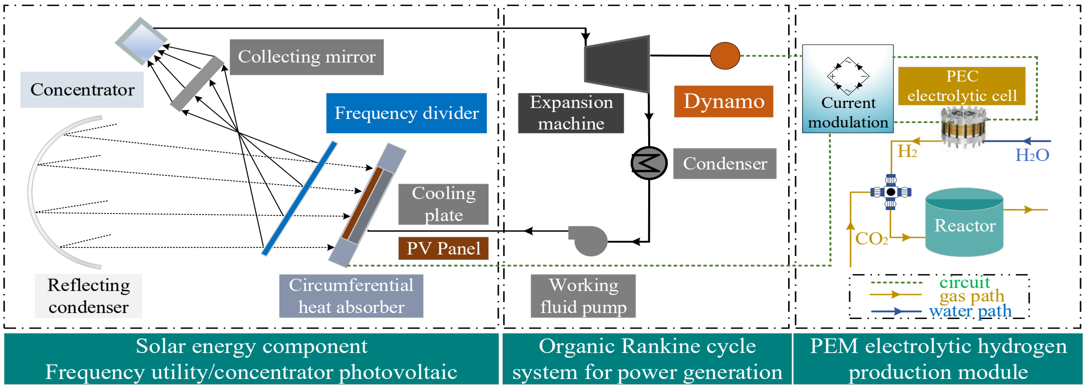

Fig. 1 Schematic diagram of integrated power supply system for full spectrum frequency division utilization of solar energy

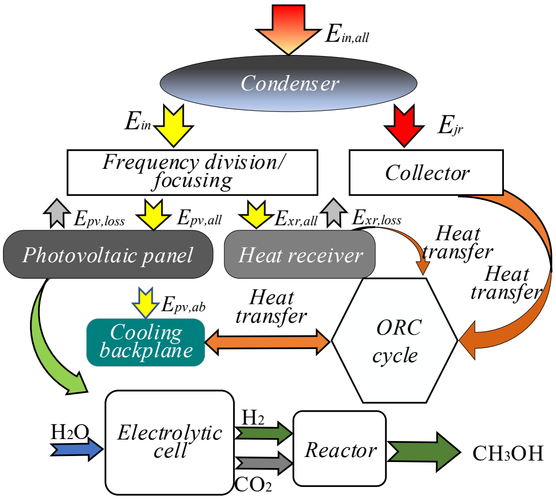

Fig 2 energy flow chart

2) ORC system: the heat of the system is provided by photovoltaic cooling backplane, circumferential heat receiver and photothermal collector, and energy conversion is realized by means of countercurrent heat exchange of organic working medium. During operation, the organic working medium is pressurized by the working medium pump and then heat exchanges with the above heat sources in turn, absorbing heat from liquid vaporization to high temperature and high pressure steam. The steam enters the expander to drive the impeller to do work. The exhaust steam is cooled and condensed into liquid in the condenser and then boosted by the working medium pump to complete the energy conversion cycle.

3) PEM electrolyzer hydrogen production module: the clean energy output by the photovoltaic panel and the electric energy generated by the expander power generation, after being processed by the high-efficiency current modulation system, provide the driving force for the PEM electrolyzer. The electrolyzer is based on proton exchange membrane (PEM) technology, which decomposes water molecules into hydrogen and oxygen under the action of direct current. The generated hydrogen and the collected carbon dioxide are transported to the thermal catalytic hydrogenation reactor together. Under the specific catalyst and optimized reaction conditions, methanol synthesis is realized through a series of catalytic reactions to build a complete green hydrogen methanol production chain.

3. Mathematical Model

3.1 Energy Flux Density Distribution

It is assumed that the energy flow density condition of solar radiation on the focal plane satisfies the Gaussian distribution [10], as shown in equation (1).

$$E = E_m e^{-\frac{r^2}{2\delta^2}} \tag{1}$$

Where E is the energy of solar radiation on the focal plane; Em is the maximum energy that can be captured; δ is the variance, which is related to the outer diameter of the heat receiver; r is the radius of the focal plane. The total energy of solar radiation on the focal plane can be obtained from equation (2).

$$E_{in,all} = \int_{r_1}^{r_2} E dr \tag{2}$$

Where $E_{\text{in,all}}$ and all are the total energy of solar radiation on the focal plane; r_1 and r_2 are the values of focal plane radius.

3.2 Energy Analysis

The total energy of the system includes the input energy of the solar photovoltaic part and the energy reflected on the collector through the frequency divider, and the expression is:

$$E_{in,all} = E_{in} + E_{jr} \tag{3}$$

Where E_{in} solar energy frequency division utilization/concentrated photovoltaic part of the input energy, E_{jr} is the energy absorbed by the collector.

The concentrated solar radiation is captured by a photovoltaic panel located in the center of the focal plane and a circular absorber. Among them, the photovoltaic panel converts part of the solar radiation absorbed into electrical energy, and the rest is lost in the form of heat; Part of the solar radiation absorbed by the heat receiver is used to heat the cooling medium of the organic Rankine cycle, and the remaining part also forms heat loss. The input energy of the above solar frequency division utilization/concentrating photovoltaic part meets the following energy balance equation, namely:

$$E_{in} = E_{pv,all} + E_{xr,all} \tag{4}$$

$$E_{pv,all} = E_{pv,ab} + E_{pv,loss} + Q \tag{5}$$

$$Q = \xi_{pv} \frac{E_{pv,all}}{\hbar} \tag{6}$$

$$\xi_{pv,J} = \xi_{pv,1}\left[1 - \alpha\left(T_{pv,m} - T_{pv,n}\right)\right] \tag{7}$$

Where: $E_{\mathrm{pv,all}}$ is the total heat absorption of photovoltaic panel; $E_{\mathrm{xr,all}}$ represents the total heat absorption of the heat absorber; $E_{\mathrm{pv,ab}}$ is the heat absorbed by the coolant of the cooling backplane; $E_{\mathrm{pv,loss}}$ is the heat loss of photovoltaic panel; Q is the electric energy generated by the photovoltaic panel; ξ_{pv} is the power generation efficiency of photovoltaic panel; $\hbar$ is the frequency division rate; $\xi_{pv,J}$ is the photovoltaic power generation efficiency when the concentration is changed to J; α is the temperature coefficient; $T_{\mathrm{pv,m}}$ and $T_{\mathrm{pv,n}}$ represent the surface temperature of photovoltaic panel and ambient temperature respectively.

The heat loss of photovoltaic panel mainly includes radiant heat loss $E_{\mathrm{loss,fs}}$ and convective heat loss $E_{\mathrm{loss,dl}}$, as follows:

$$E_{loss,fs} = \varepsilon\sigma\left(T_{pv,m}^4 - T_0^4\right)S_{pv} \tag{8}$$

$$E_{loss,\mathrm{dl}} = h\left(T_{pv,m} - T_0\right)S_{pv} \tag{9}$$

Where ε is the surface radiation coefficient of the photovoltaic panel, σ is the blackbody radiation constant, S_{pv} is the area of the photovoltaic panel, h is the convection heat transfer coefficient of the photovoltaic panel, T_0 is the ambient temperature, $T_{\mathrm{pv,m}}$ is the surface temperature of the photovoltaic panel. It can be seen from (8) and (9) that when the concentration ratio is 500, $E_{\mathrm{pv,loss}}/E_{\mathrm{pv,all}}$ are the thousandth ratio, so the heat loss of the photovoltaic panel can be ignored.

The energy conservation of the annular absorber is expressed as follows:

$$E_{xr,all} = E_{xr,ab} + E_{xr,loss} \tag{10}$$

Where: $E_{\mathrm{xr,all}}$ are the total heat of the circumferential heat receiver, $E_{\mathrm{xr,ab}}$ are the heat absorbed by the circumferential heat receiver, $E_{\mathrm{xr,loss}}$ are the heat loss of the circumferential heat receiver.

Assuming that the heat loss only comes from the surface of the heat receiver, other surfaces can be well insulated, and the corresponding heat transfer loss is very small. The heat loss $E_{\mathrm{xr,loss}}$ on the surface of the heat receiver mainly include convective heat loss $E_{\mathrm{loss,dl}}$, radiant heat loss $E_{\mathrm{loss,fs}}$ and reflected heat loss $E_{\mathrm{loss,fs'}}$.

$$E_{xr,loss}=E_{loss,dl}+E_{loss,fs}+E_{loss,fs'} \tag{11}$$

$$E_{loss,dl}=h_v\times(T_{xr,m}-T_0)\times S_{xr} \tag{12}$$

$$E_{loss,fs}=\mu\times\sigma\times(T_{xr,m}^4-T_1^4)\times S_{xr} \tag{13}$$

$$E_{loss,fs'}=E_{\mathrm{xr}}\times\tau \tag{14}$$

Where: h_v is the convective heat transfer coefficient of the heat receiver, S_{xr} is the area of the heat receiver, T_1 is the atmospheric temperature, μ is the surface radiation coefficient of the heat receiver, and τ is the reflectivity of the heat receiver.

4. Photovoltaic Array Fault Detection

During the entire lifecycle of photovoltaic systems, defects such as cracks, punctures,and hidden cracks are prone to occur during production, transportation, and long-term operation, leading to a decrease in the photovoltaic conversion efficiency of components. Studies have shown that the annual cost loss caused by failures can reach up to 18.9% [11-12].

In the current online fault diagnosis of photovoltaic modules, artificial intelligence models have become a research focus due to their outstanding advantages in extracting complex fault features. The improved ANN photovoltaic fault diagnosis model proposed in this article introduces gate controlled convolutional layers and flattening layers in the input-output layers, replaces traditional hidden layers with a double-layer fully connected structure, and optimizes the output layer using Adaptive Sofmax activation function. The gated convolutional layer combines the advantages of GRU and CNN, with the convolution part extracting spatial features and the gating part retaining the update and reset gates of GRU, efficiently capturing temporal information and avoiding gradient vanishing, adapting to the data characteristics of photovoltaic systems. Through simulation and on-site data verification, the model outperforms mainstream algorithms such as KNN[13]and LSTM[14]in terms of fault diagnosis accuracy and generalization ability.

The gating mechanism achieves dynamic filtering of convolution generated features through the collaboration of update gates and reset gates: the update gate adjusts the fusion ratio between historical information and the current input,while the reset gate controls the degree of forgetting of historical information. By selectively retaining key features and filtering out noise interference, both significantly improve the model's ability to express and generalize complex fault features. Finally, through the output propagation process, effective features are integrated to provide high-quality feature representations for subsequent fault diagnosis.The process is as follows.

$$i_k = \tau\left(M_i \cdot \left[\ell_{k-1},\ m_k\right] + \hbar_i\right) \tag{15}$$

$$j_k = \tau\left(M_j \cdot \left[\ell_{k-1},\ m_k\right] + \hbar_j\right) \tag{16}$$

$$\ell_k = j_k * \ell_{k-1} + \left(1 - j_k\right) * \tilde{\ell}_k \tag{17}$$

Where i_k represents the output of the reset gate (value between 0 and 1), τ represents the sigmoid function, M_i and M_j represent the weight matrix corresponding to the reset gate and update gate, $\ell_{k\text{-}1}$ represents the hidden state of the previous time step, m_k represents the input of the current time step, $\hbar_i$ and $\hbar_j$ represent the offset term of the reset gate and update gate, j_k represents the output of the update gate (value between 0 and 1), ℓ_k represents the hidden state of the current time step, * represents the element level multiplication, and $\tilde{\ell}_k$ is the candidate hidden state.

Gated convolutional network is defined as:

$$Conv1 = \sum\sum F_m \cdot C \tag{18}$$

$$Conv2 = \sum\sum F_n \cdot C \tag{19}$$

$$W = Conv1 \otimes Sigmoid(Conv2) \tag{20}$$

Where F is the convolution filter, C is the channel value of the convolution kernelat the characteristic position, W is the gated convolution network output, *Conv* is the convolution layer, and *sigmoid* is the gating unit function.

Through the gated convolution layer, the two-dimensional feature mapping is obtained, and the two-dimensional array mapping is reduced to one dimension and output by using the flatten layer, which greatly reduces the redundant parameters of the network structure. The formula is expressed as:

$$Flatten\left(array\left(\left[\left[x_{11} \cdots x_{1n}\right], \cdots \left[x_{m1} \cdots x_{mn}\right]\right]\right)\right) = array\left(\left[x_{11} \cdots x_{1n} \cdots x_{m1} \cdots x_{mn}\right]\right) \tag{21}$$

When classifying different states, several full connection layers can be added. Based on the actual situation, two fully connected layers are selected, and the formula is as follows:

$$y = f\left(\sum_{m=1}^{N} \varpi_m x_m + \psi\right) \tag{22}$$

Where $f(\cdot)$ is the activation function, y is the integrated output characteristic, x_m is the input characteristic, and ϖ and ψ are the weight parameters and bias respectively. Relu is selected as the activation function of the full connection layer.

4.1 Adaptive Softmax

Using Adaptive sofmax as the classifier of the improved ANNfault diagnosis model can effectively reduce the impact of the increase in computing time due to the large size of the data set without affecting the accuracy. The specific method is to divide the word dictionary V to be classified into two clusters according to the frequency of word occurrence. Given a vocabulary containing ℓ words, first find the number ℓ_h assigned to the first cluster word, which will cover the χ_k value of the distribution. The tail cluster will contain the rest of the vocabulary, consisting of $\ell_k = \ell - \ell_h$ words, covering the $\chi_k = 1 - \chi_h$ of the overall distribution. The calculation time of matrix multiplication corresponding to the root is equal to $\varphi(\ell_h + 1, D)$, and the calculation time of the tail of the distribution is equal to $\varphi(\ell_k, \chi_k D)$, where D is batch, and the total calculation time is:

$$Q = \varphi(\ell_h + 1, D) + \varphi(\ell_k, \chi_k D) \tag{23}$$

4.2 Fault Diagnosis Process

The PV array fault diagnosis process is carried out around data processing, model training, model evaluation and verification, as shown in Fig 3. The specific contents are as follows:

1) Data acquisition and preprocessing: first, obtain the status data of PV array in normal operation and various fault conditions. In order to eliminate the influence of dimensional difference of data on subsequent analysis, the collected data are normalized. The processed data constitutes a sample set, and is divided into training samples and test samples according to a specific proportion. Training samples are used to learn model parameters, and test samples are used to evaluate model performance.

2) Model training and Parameter Optimization: input the training sample set into the improved ANN model. The data enters the model through the input layer, and the depth feature is extracted through the gated convolution layer. Then the feature classification is completed by the full connection layer, and finally the classification results are output at the output layer. In the training process, the iterative optimization method is used to dynamically adjust the number of filters, convolution kernel size of the gated convolution layer, and the number of neurons in the full connection layer and other key parameters, so that the model achieves the best fitting effect on the training set.

3) Model evaluation and validation: after the training, input the test sample set into the trained improved ANN model. The model processes the test samples and outputs the fault diagnosis results. By comparing the actual fault types with the model diagnosis results, the accuracy, recall and other evaluation indicators are used to comprehensively evaluate the fault diagnosis performance of the model. If the evaluation results meet the preset criteria, it indicates that the model is effective. By now, the model is established and can be put into practical application; If the requirements are not met, it is necessary to return to adjust the model parameters and conduct training and evaluation again.

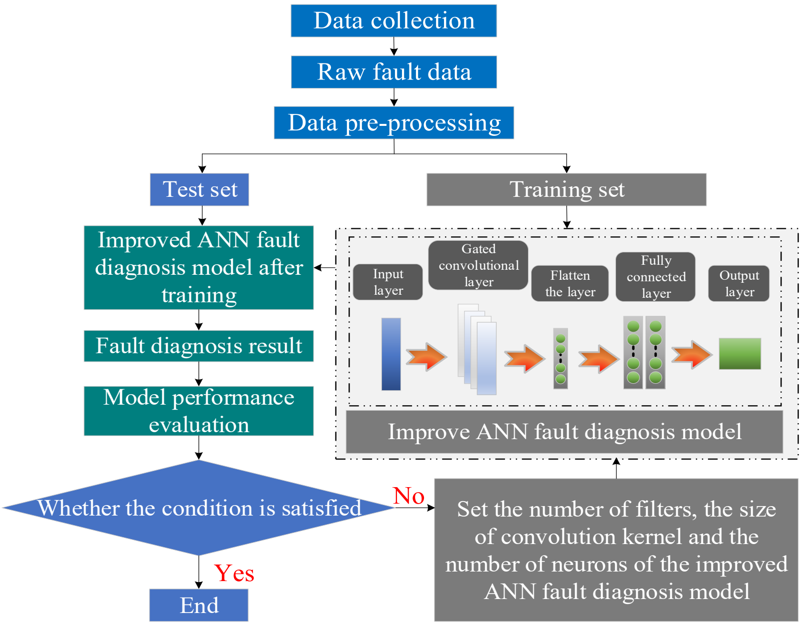

Fig 3 fault diagnosis flow chart

5. Results and Discussion

The main parameters of the system used are shown in Table 1.

Table 1

Main parameters of the system

Parameters	Numerical Value
Variance δ	0.8m
Photovoltaic panel power generation efficiency ξ_{pv}	0.34
Fractional frequency $\hbar$	0.889
Temperature coefficient α	$0.002K^{-1}$
Surface radiation coefficient of PV panelε	0.85
Blackbody radiation constant σ	$5.67\times10^{-8}W/(m^2\cdot K^4)$
The convective heat transfer coefficient of photovoltaic panels h	$10\ V/(m^2\cdot K)$
The convective heat transfer coefficient of the heat absorber h_v	5.7+3.8v
wind speed v	5m/s
free air temperature T_1	$0.552T_0^{1.5}$
Surface radiation coefficient of the heat absorberμ	0.85
Reflectivity of heat absorber τ	0.05
Pinch point temperature difference $T_{\Delta T}$	10K
The relaxation coefficient γ	0.8

5.1 Determination of ORC Working Medium and Evaporation Temperature

In this study, the heat energy of solar constant temperature process is used as the heat source of the system, and the pure working fluid is selected as the research object. The characteristic parameters of the three experimental refrigerants shown in Table 2 include ozone depletion potential (ODP) and global warming potential (GWP). Under the condition that the temperature of the cooling backplane is constant at 100 ℃, set three evaporation temperatures of 70 ℃, 80 ℃ and 90 ℃ (in steps of 10K) to explore the influence of working medium and evaporation temperature on the system performance. The results are shown in Fig.4 and Fig. 5.

Table 2

Working fluid physical parameters

working fluids	molar mass/ (kg•kmol-1)	critical pressure/MPa	critical temperature/℃	ODP	GWP
R601a	72.15	3.38	187.20	0	0.001
R134a	102.03	4.06	101.06	0	0.130
isobutene	56.11	4.01	144.94		

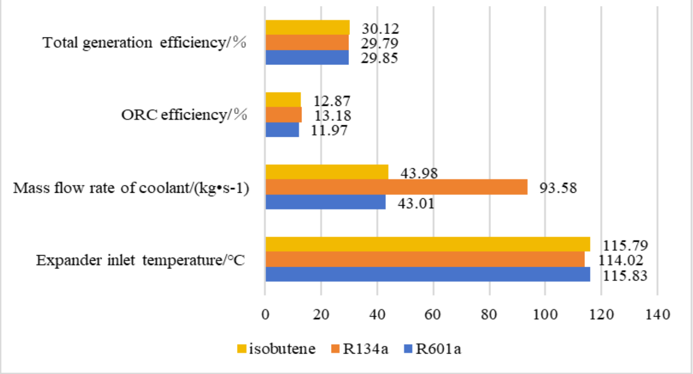

Fig.4 performance comparison of three working fluids

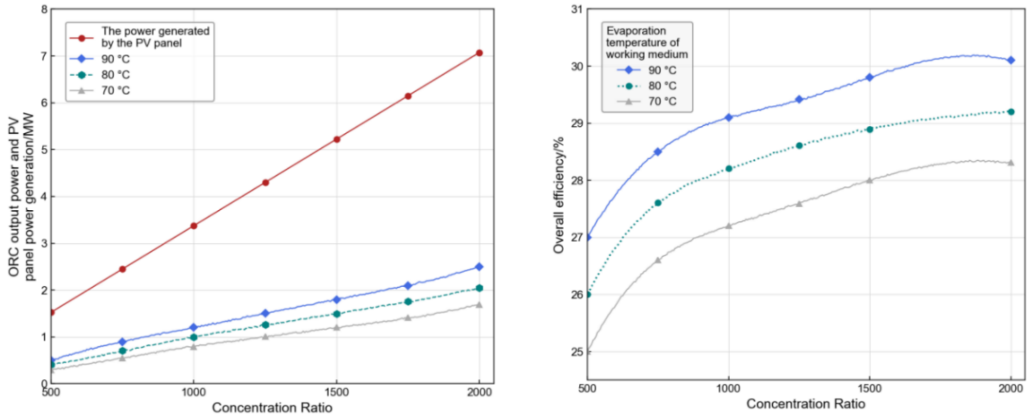

（1） System power （2） overall efficiency

Fig.5 The influence of working fluid evaporation temperature on system performance

Fig. 5 (1) shows that the output power of ORC and the power generated by photovoltaic panels increase as a whole when the concentration ratio increases from

500 to 2000. When the working medium evaporation temperature is 90°C and the concentration ratio reaches 2000, the ORC net output power reaches the maximum value of 2.70MW; the photovoltaic panel power generation is strictly proportional to the concentration ratio, which is not affected by the evaporation temperature, and the maximum value is 7.09 MW. Fig 5 (2) shows that under different concentration ratios, the total power generation efficiency of the system increases with the increase of the working medium evaporation temperature. For every 10K increase in the evaporation temperature, the total efficiency of the system increases by about 1%, which determines that 90°C is the evaporation temperature calculated for subsequent working conditions. In addition, the improvement of the concentration ratio can increase the overall efficiency of the system, with a maximum increase of 2.84%. The experimental data in Fig 5 shows that the system performance corresponding to isobutene working fluid is the best under the conditions of 2000 condensing ratio, 90°C evaporation temperature and saturated steam at the PV panel outlet.

5.2Analysis of ORC Output Performance

Fig.6 shows the change of thermal efficiency of ORC system with working medium mass flow. The figure shows that there is an optimal working fluid mass flow for each condensing ratio, which maximizes the thermal efficiency of the ORC system. At the same time, the thermal efficiency of the system has little difference under different working fluid mass flow rates, which are maintained at 12.98%~13.02%. Combined with the thermal efficiency of ORC system, it can be estimated that the contribution of ORC system to the power generation of the whole coupled energy system is about 9%.

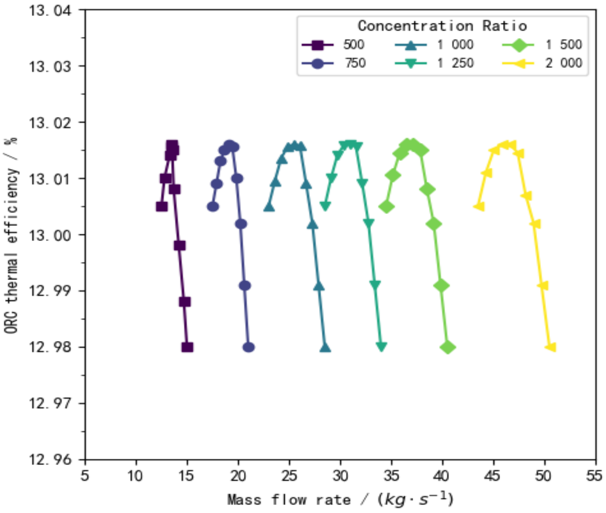

Fig. 6shows the change of thermal efficiency of ORC system with working medium mass flow

5.3 Performance Simulation of Photovoltaic Array Fault Detection

The photovoltaic module of LONGi Green Energy Technology Co._Ltd. LR6-72PH-350M is selected in matlab/simulink software. The module parameters are: maximum power point voltage 38.8V, maximum power point current 9.03A, open circuit voltage 47.5V, short circuit current 9.57A. The photovoltaic array simulation model of 4 × 4 array is established, as shown in Fig 7.

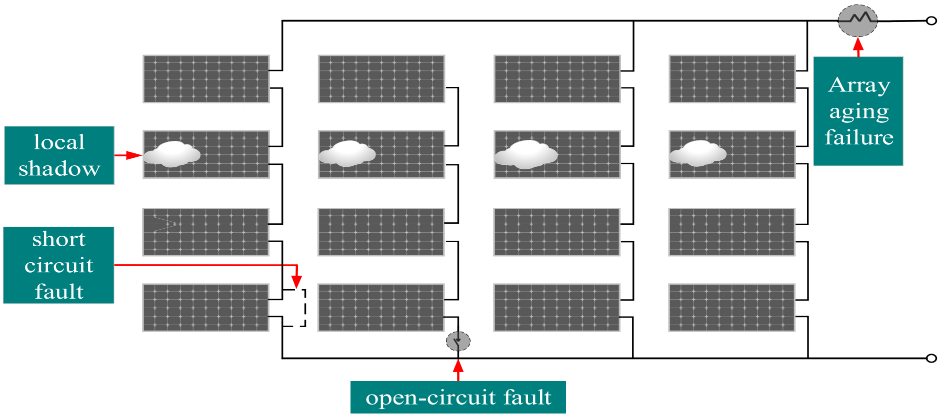

Fig7 Photovoltaic array simulation model

5.4 Fault Diagnosis Test

Table3

Simulate data set running labels, status, and quantity

Label	Operation status description	number
0	normal operation	300
1	Short circuit: one and two photovoltaic templates are respectively set with 300 groups of data	600
2	Aging: connect the same branch to three different levels of resistors in turn, and obtain 300 groups of data respectively	900
3	Local open circuit: set one branch open circuit and two branch open circuits respectively, with 300 groups of data for each	600
4	Dirt shielding: reduce the irradiance of one and two photovoltaic modules of a branch, 300 groups of data each	600
5	Shadow occlusion: reduce the irradiance of the entire photovoltaic array	300
6	Open circuit dirt fault	300

In the photovoltaic system simulation model, in order to cover a variety of operating environments, the input irradiance range is set to 100-1000w/m^2, the change step is 50w/m^2, the temperature range is set to 10-48°C, and the change step is 2°C through the constant module in Matlab/Simulink software. Five single line faults are simulated: short circuit, aging, partial open circuit and dirt shielding; 1 parallel fault: open circuit dirt fault [15]. In the simulation experiment, goto, soope and from modules are used to obtain data. Each group of data (temperature, short-circuit current, open circuit voltage, irradiance, working current and working voltage values and status labels) constitute a sample, and multiple groups of different experiments are conducted to form a complete data set. The simulation process of various operating states in the dataset is shown in Table3.

Due to the large differences in the numerical values of different types of data in the data sets simulated above, which leads to the decline of the accuracy of model fault diagnosis and generalization ability, in order to better train the improved artificial neural network model, the data sets obtained above are normalized [16], and the normalization formula is shown in equation 29.

$$X = \{x_i\} = \frac{x_i - x_{\min}}{x_{\max} - x_{\min}} \tag{24}$$

Where x_i is the original input data, $x_{\min}$ and $x_{\max}$ are the minimum and maximum values in the original data, and X is the input data after normalization.

In order to better verify the effectiveness of the improved Ann fault diagnosis model, 60% of the above data sets were randomly selected as the training set and 40% as the test set. ACC is introduced to indicate the overall accuracy, and P is the accuracy of a single fault. Recall indicates the recall rate, F1 indicates the harmonic average value, and the improved Ann diagnostic model is evaluated. The mixed matrix of index calculation is shown in Table4.

Table 4

The mixed matrix of index calculation

Confusion matrix		Forecast Sample	
		Positive	Negativ
Actual sample	Positive	True Positive （TP）	False Negativ （FN）
	Negativ	False Positive （FP）	True Negative （TN）

$$ACC = \frac{TP + TN}{TP + TN + FN + FP} \tag{25}$$

$$P = \frac{TP}{TP + FP} \tag{26}$$

$$recall = \frac{TP}{TP + FN} \tag{27}$$

$$F1 = \frac{2 \times precision \times recall}{precision + recall} \tag{28}$$

Set the input data shape of the model input layer (6, 1); 16 filters are selected for gated convolution layer, the convolution kernel is 3, and the activation function is relu; The number of neurons in the whole connective layer (1,2) was 8, the initialization was evenly distributed, and the activation function was relu; The number of neurons in the output layer is 8, and the activation function is adaptive softmax. As shown in Fig8, the fault diagnosis model has excellent performance.

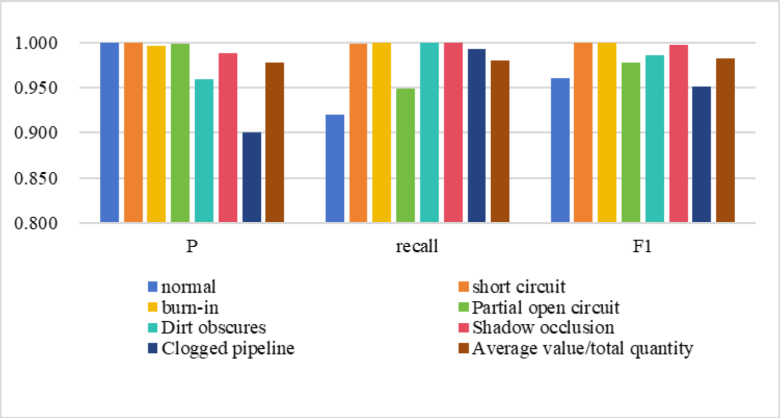

Fig.8 fault diagnosis

5.5 Comparative Test

To further verify the diagnostic performance of the improved model, the two PV diagnostic models, KNN and LSTM, are used as comparative diagnostic models. The training set and test set shown in Table 4 are used for model training and diagnostic performance testing. The multi classification confusion matrix of the three models for seven types of states on the test set is shown in Fig 9, and the accuracy is shown in Fig 10.

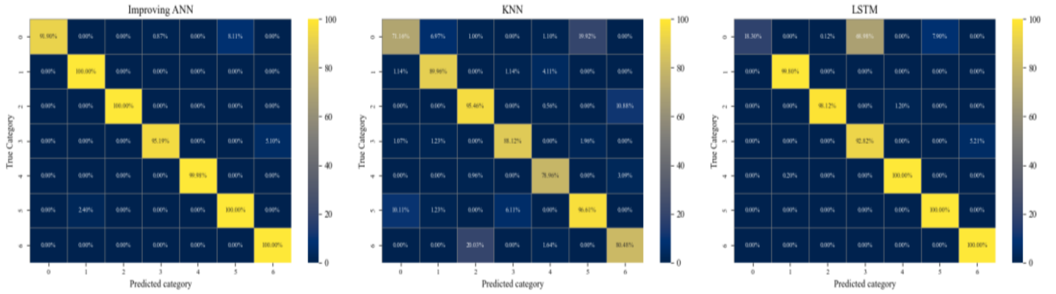

Fig.9 Three models of confusion matrix comparison

From the confusion matrix, it can be seen that due to the fact that the characteristics of slight aging and slight fouling are not obvious relative to the normal operation state during fault simulation, the comparison model is not easy to distinguish the two types of faults, aging and fouling blocking, from the normal state, and also does not distinguish the open dirt from the partial Road, while the improved Ann fault diagnosis model can distinguish these five types of situations well. In the test set, the improved ANN model only misclassifies a small amount of data of normal state, local open circuit, shadow occlusion and open circuit dirt, and the classification accuracy of other samples is 100%. It can be seen from Fig 14 that the improved ANN model has higher accuracy in the simulated data set than the other two models, which proves the superiority of the improved Ann fault diagnosis model.

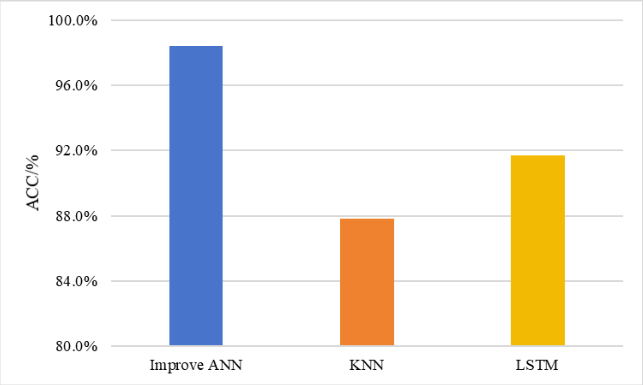

Fig.10 Accuracy rate

6. Conclusion

In this paper, a new type of solar energy comprehensive utilization system is proposed based on the full spectrum cascade efficient utilization of solar energy and the integration of frequency division technology and concentrated photovoltaic solar thermal hybrid system, and theoretical modeling and thermodynamic analysis are carried out; At the same time, the ANN method is innovated and improved for photovoltaic module fault detection. Through systematic research, the following conclusions are drawn:

(1) In terms of performance optimization of solar energy comprehensive utilization system, it is found that there is a matching relationship between the concentration ratio and the working fluid mass flow, and each concentration ratio corresponds to an optimal working fluid mass flow, which can make the ORC system obtain the maximum thermal efficiency. It is worth noting that the thermal efficiency of the system fluctuates slightly under different working medium mass flows, and is basically stable at about 13%. It is estimated that the ORC system contributes about 9% to the power generation of the whole coupled energy system.

(2) In the photovoltaic array fault detection technology innovation, the ANN model is optimized. A gated convolution layer, a flattening layer and two full connection layers are introduced between the input layer and the output layer to replace the traditional hidden layer, which significantly improves the diagnostic performance of the model. Based on MATLAB simulation data set, the improved ANN model is compared with KNN and LSTM models. The results show that the diagnosis accuracy of the improved ANN model is as high as 98.6%, which shows better diagnosis performance than the comparison model.

Acknowledgments:

This work was supported by Lanzhou University of Technology Innovation Training Program for College Students (Grant No. DC20250859)

REFERENCES

[1] *LIHong , LYUPengxiao, LIQiang* , et al. A Review of Performance Studies and Improvement Measurements Concerning Solar Photovoltaic and Thermal Collectors. Building science. Vol. **42**, Iss. 2, 2025.

[2] *IEA.* World Energy Outlook 2024. Paris: International Energy Agency, 2025.

[3] *ZHANG Manzheng, GUO Wei, FANG Yuche*ng, et al. Thermodynamic Analysis of a Photovoltaic/Photothermal Integrated Power Generation System Based on Solar Energy Spectrum Utilization. Journal of Chinese Society of Power Engineering, Vol.**44**, Iss. 8, 2024.

[4] *Zheng X, Zhou Y. A* three-dimensional unsteady numerical model on a novel aerogel-based PV/T-PCM system with dynamic heat-transfer mechanism and solar energy harvesting analysis. Applied Energy, 2023, 338.DOI: 10.1016/j.apenergy.2023.120899.

[5] *WOLF M.* Perforance analyses of combined heating and photovoltaic power systems for residences. Energy Conversion, Vol. **16**, Iss. 1-2 1976.

[6] *WANG Xiuyan, HAN Lu.* Study on heat-transfer characteristics of a parabolic trough solar collector. Journal of Chinese Society of Power Engineering. Vol.**37**, Iss. 4.2017.

[7] *LI Z, JI J, YUAN W, et al.* Experimental and numerical investigations on the performance of a G-PV/T system comparing with A-PV/T system. Energy, 2020.

[8] *CHAE S, BAE S, NAM Y.* Economic and environmental analysis of the optimum design for the integrated system with air source heat pump and PVT. Case studies in thermal engineering,2023,48:103142.

[9] *Xiang Yuyue, Chu Leichi, Fang Yuan, et al.* Experimental Study of PV/T- Based Dual-Source Heat Pump Water Heater. Acta energiae solaris sinica, Vol. **45**, Iss. 10 2024.

[10] *Xu P P,* Research on heat receiver thermal performance of solar thermal power tower plant. Hangzhou. Zhejiang University, 2015.

[11] *Hichri A, Halji M, Mansouri M, et al.* Genetic-algorithm-based neural network for fault detection and diagnosis: Application to grid-connected photovoltaic systems. Sustainability, Vol. **14**, Iss. 17, 2022.

[12] *Venkatakrishnan G R, Rengaraj R, Tamilselvi S, et al.* Detection, location, and diagnosis of different faults in large solar PV system-a review. International Journal of Low-Carbon Technologies, Vol. **18**,2023.

[13] *Madeti S R, Singh S N.* Modeling of PV system based on experimental data for fault detection using kNN method. Solar Energy, Vol. **173**, 2018.

[14] *Appiah A Y, Zhang X, Ayawli B B K, et al.* Long short-term memory networks based automatic feature extraction for photovoltaic array fault diagnosis. IEEE Access, Vol.**7**, 2019.

[15] *Chen Shiqun, Yang Gengjie, Gao Wei.* A fault diagnosis method for photovoltaic array via BOA-SAE-EELM. Acta Energiae Solaris Sinica, Vol. **43**, Iss.4,2022.

[16] *Qian Liang, Huang Wei, Yang Jian wei.* Research on fault diagnosis method of photovoltaic array based on HHO-ELM. Chinese Journal of Power Sources, Vol. **48**, Iss. 2,2024.